International Journal of Biochemistry and Cell Biology 114 (2019) 105561

Contents lists available at ScienceDirect

International Journal of Biochemistry and Cell Biology

journal homepage: www.elsevier.com/locate/biocel

Antimony, a novel nerve poison, triggers neuronal autophagic death via reactive oxygen species-mediated inhibition of the protein kinase B/mammalian target of rapamycin pathway

Xiaoke Wang[a,1], Piaoyu Zhu[a,1], Shenya Xu[a], Yuting Liu[a], Yang Jin[a], Shali Yu[a], Haiyan Wei[a], Jinlong Li[b], Qinglin Zhang[c], Takahiro Hasegawa[d], Chenjuan Yao[d], Hiroshi Yoshimura[d], Qiyun Wu[e], Xinyuan Zhao[a,*]

[a] Department of Occupational Medicine and Environmental Toxicology, School of Public Health, Nangtong University, Nantong, 226019, China
[b] School of Pharmacy, Nantong University, Nantong, 226001, China
[c] Departments of Gastroenterology, Wuxi People's Hospital Affiliated to Nanjing Medical University, Wuxi, 214023, China
[d] Department of Molecular Oral Physiology, Institute of Biomedical Sciences, Tokushima University Graduate School, 770-8504, Japan
[e] Department of Nutrition and Food Hygiene, School of Public Health, Nangtong University, Nantong, 226019, China

ARTICLE INFO

Keywords:
Antimony
Neurotoxicity
Autophagy
Akt/mTOR inhibition
Neuronal apoptosis
ROS

ABSTRACT

Antimony (Sb), a naturally occurring metal present in air and drinking water, has been found in the human brain, and there is evidence of its toxic effects on neurobehavioral perturbations, suggesting that Sb is a potential nerve poison. Here, we provide the first study on the molecular mechanism underlying Sb-associated neurotoxicity. Mice exposed to antimony potassium tartrate hydrate showed significantly increased neuronal apoptosis. *In vitro*, Sb triggered apoptosis in PC12 cells in a dose-dependent manner. Mechanically, Sb triggered autophagy as indicated by increased expression of microtubule-associated protein 1 light chain 3-II (LC3-II) and accumulation of green fluorescent protein-tagged LC3 dots. Moreover, Sb enhanced autophagic flux and sequestosome 1 (p62) degradation. Subsequent analyses showed that Sb treatment decreased phosphorylation of protein kinase B (Akt) as well as the mammalian target of rapamycin (mTOR), while an Akt activator protected PC12 cells from autophagy. Moreover, the antioxidant *N*-acetylcysteine attenuated Sb-induced Akt/mTOR inhibition and decreased autophagy and apoptosis, with autophagy inhibition also playing a cytoprotective role. *In vivo*, mice treated with Sb showed higher expression of LC3-II and p62 in the brain, consistent with the *in vitro* results. In summary, Sb induced autophagic cell death through reactive oxygen species-mediated inhibition of the Akt/mTOR pathway.

1. Introduction

Humans are exposed to antimony (Sb) in the natural environment through the air as well as by water (Herath et al., 2017). Occupational exposure to Sb occurs in workers associated with industries producing Sb, metal mining, or smelting and refining. Sb is also used as a drug for the treatment of schistosomiasis and leishmaniasis. Following Sb exposure, the two most important health effects involve the respiratory and cardiovascular systems (Sundar and Chakravarty, 2010). Several decades ago, researchers also reported the presence of Sb in the human brain (Hock et al., 1975). Tanu et al. have recently reported that Sb enters and accumulates in the mouse brain after intraperitoneal injection, which leads to impaired cognitive function as determined by the Morris water maze (Tanu et al., 2018). However, it is unknown how Sb induces neurological effects leading to impairment of learning and memory.

Alzheimer's disease (AD) is the most prevalent neurodegenerative disease, involving massive loss in areas of the brain responsible for memory and learning. It is characterised by two molecular hallmarks, namely the deposition of extracellular plaques of β-amyloid protein (Aβ) and intracellular neurofibrillary tangles (Polanco et al., 2018). Although there has been a great deal of research into the causes and consequences of AD, many aspects of the disorder still remain unclear. Among the mechanisms of AD pathogenesis, neuronal cell death may be

* Corresponding author.
E-mail address: zhaoxinyuan@ntu.edu.cn (X. Zhao).
[1] These authors contributed equally to this work.

https://doi.org/10.1016/j.biocel.2019.105561
Received 9 February 2019; Received in revised form 30 April 2019; Accepted 19 June 2019
Available online 20 June 2019
1357-2725/

an important phenomenon as shown by the following: 1) both Aβ deposition and tau phosphorylation induce neuronal death (Cho et al., 2017; Kayed and Lasagna-Reeves, 2013); 2) massive neuronal cell death contributes to morphological changes in AD including a dramatic shrinkage in cortical volume (Fricker et al., 2018); 3) more TUNEL-positive cells were found in AD cases compared with normal brains (Smale et al., 1995). Some environmental stimuli can induce neuronal cell death, therefore contributing to the risk of neurodegeneration. Epidemiological studies have provided an association between several heavy metals and AD, including lead, cadmium, and arsenic (Fathabadi et al., 2018; Xu et al., 2018; Yang et al., 2018). Not surprisingly, all of them triggered neuronal cell death. For example, lead, a classic nerve poison, leads to neuronal death both in *vitro* and in *vivo* (Dribben et al., 2011; Engstrom et al., 2015). Neuronal cell death, as an important indicator of neurological toxicity, is shared by heavy metals (Cariccio et al., 2018; Morris and Levenson, 2017). Until now, there have been no experimental data for neuronal death induced by Sb. We therefore first characterised Sb-induced neuronal cell death, to provide basic evidence of Sb-associated neurotoxicity.

Macroautophagy, hereafter called autophagy, is a "self-eating" process, which involves the engulfing of cytoplasmic proteins or organelles into autophagosomes, followed by fusion with lysosomes and subsequent degradation. Recently, our group provided the first evidence of an association between autophagy and Sb-induced toxicity. We showed that Sb stimulated a loss of cell viability *via* reactive oxygen species (ROS)-dependent autophagy in the A549 alveolar epithelial cell line (Zhao et al., 2017). Autophagy normally acts as a survival mechanism to prevent neuronal cell death, but excessive autophagy can lead to death (Fricker et al., 2018). Defects in autophagy likely contribute to the pathogenesis of numerous neurodegenerative diseases, including AD (Zare-Shahabadi et al., 2015). Emerging evidence has demonstrated that an alteration in the autophagic pathway may be related to the onset of environmental pollutants (*e.g.*, metal or other chemical-associated neurotoxicity) (Pellacani and Costa, 2018). Additionally, Zhang et al. reported that an excessive increase of autophagy induced by lead may lead to autophagic cell death and subsequent neurotoxicity (Zhang et al., 2012). Can Sb induce neuronal cell autophagy and death? What are the molecular mechanisms underlying Sb-induced autophagy in neuronal cell lines and brain tissue? Is autophagy a positive or negative factor during Sb-triggered neuronal cell death?

The present study addresses these questions, both *in vitro* and *in vivo*. The results demonstrated in detail that Sb activated autophagy through ROS-mediated Akt/mTOR pathway inhibition. Moreover, autophagic flux was enhanced, although p62 expression was increased rather than decreased, while inhibition of autophagy attenuated Sb-induced neuronal cell apoptosis. Our findings provide the first evidence that Sb induces autophagic cell death in neuronal cells, thus identifying the first molecular mechanism of Sb-induced neurotoxicity, involving Sb as a novel nerve poison.

2. Materials and methods

2.1. Plasmids, reagents and antibodies

The plasmids GFP-LC3 was a gift from Dr. Wei Liu (Department of Biochemistry and Molecular Biology; Zhejiang University School of medicine). The chemicals rapamycin (R8781), chloroquine (CQ) (C6628), potassium antimonyl tartrate trihydrate (60,063), N-acetylcysteine (NAC, 1,009,005), 3-methyladenine (M9281), cycloheximide (C4859), Hoechst (94,403) were purchased from Sigma-Aldrich. Akt activator was from TargetMol (T2274).

The primary antibodies were used as follows: anti-LC3B (Sigma, L7543), anti-p62 (Sigma, P0067), anti-ACTB (Sigma, A5316), anti-mTOR (CST, 2972), anti-p-mTOR (CST, 2971), anti-Akt (CST, 4685), anti-p-Akt (CST, 4060), anti-c-c3 (CST, 9664), anti-GFAP (CST, 12,389), anti-NeuN (Proteintech, 26975-1-AP)

2.2. Cell culture, treatment and transfection

The rat pheochromocytoma neuro cell line PC12 (from Shanghai Cell Bank, Chinese Academy of Sciences) were cultured in Dulbecco's modified Eagle's medium (DMEM, GIBCO, Shanghai, China) supplemented with 10% fetal bovine serum (FBS) at 37 °C in a humidified atmosphere with 95% air and 5% CO_2. To control mycoplasma, the detection is performed at least once a week as an obligatory quality control cell culture experiment. We use direct PCR protocol which allows detection of a range of mollicutes including *Mycoplasma gallisepticum* and Mycoplasma synoviaeto. After cell seeding and incubation for 24 h, the Sb dissolved in saline (0.9% NaCl) were added into cell culture medium. The final saline conten in culture medium was 0.5% (v/v), and backgroup control wells were treated with only 0.5% saline. DNA Transfection Reagent (Lipofectamine 2000, Invitrogen) was used for plasmid transfection according to manufacturer's instruction.

2.3. Animal treatment

All animal experiments were performed according to the ethical guidelines by the Ethics Committee of Laboratory Animal Care and Welfare, Nantong University School of Medicine. The ICR male mice (average body weight 25–30 g, 6-week old) were from the animal center of Nantong University, and acclimated for one week on a 12/12 h dark/light cycle. After acclimatization, mice were divided into four groups: control (0.9% normal saline) and Sb exposed group (10, 20, 40 mg/kg). Mice were exposed to 100 μl Sb through intraperitoneal injection at different doses three times per week for 4 weeks before harvest. All experimental mice had free access to water and food.

2.4. CCK-8 analysis

PC12 cells were plated at a density of 10×10^3 cells/well in 96 well plates, and the cell viability was assessed by the cell counting kit-8 assay (Dojindo Laboratories, Japan) according to the manufacturer's instruction. Briefly, after Sb treatment, CCK-8 solution was added to each well of the plate and the cells were incubated for another 2 h, and the absorbance was measured at 450 nm on an automated reader (Bio-Tec, City, CA, USA).

2.5. Intracellular ROS assay

The level of intracellular ROS was measured using a fluorescent probe DCFH-DA (Beyotime, China). It is a cell-permeable non-fluorescent probe, and de-esterified intracellularly and turns to highly fluorescent 2′,7′-dichlorofluorescein upon oxidation. In brief, after treatment with Sb at different concentrations for 24 h, the PC12 cells were incubated with serum-free medium including 10 μM DCFH-DA probe. After rinsing with PBS 3 times to elimminate excess probe, the fluorescence intensity was detected at 525 nm using a microplate reader.

2.6. Reverse transcription-polymerase chain reaction (RT-PCR) and Quantitative real-time polymerase chain reation (qRT-PCR) analysis

Total RNA from PC12 cells was extracted with Trizol reagent (Invitrogen, Shanghai, China) according to the manufacturer's instructions. Extracted RNA was reverse transcribed for cDNA synthesis using Omniscript RT-PCR kit (Qiagen, Germany) in accordance with the manufacturer's protocol. The cDNA was amplified using the Table1 primers. The PCR products for each sample were analyzed by electrophoresis in a 1.5% agarose gel. Gels were stained with ethidium bromide and analyzed under ultraviolet light. The intensity of the mRNA expression was measured by densitometry and then corrected with the corresponding β-actin mRNA measurement. For qRT-PCR, PCR analysis was performed in 10 μL reactions using SYBR GREEN PCR Master Mix

Table 1
DNA sequences of primers for polymerase chain reaction.

Gene name	Primer name	Sequence
RAT *β-actin*	R-ACTB-F	5'-CTCCGGAGTCCATCACAATG-3'
	R-ACTB-R	5'-CTACAATGAGCTGCGTGTGG-3'
RAT *p62*	R-*p62*-F	5'-GGTGTCTGTGAGAGGACGAGGAG-3'
	R-*p62*-R	5'-TCTGGTGATGGAGCCTCTTACTGG-3'
RAT *Atg5*	R-*Atg5*-F	5'-CTCAGCTCTGCCTTGGAACATCAC-3'
	R-*Atg5*-R	5'-AAGTGAGCCTCAACTGCATCCTTG-3'
RAT *Atg7*	R-*Atg7*-F	5'-GTGAACCTCAGCGGATGTATGGAC-3'
	R-*Atg7*-R	5'-CCAGCAGCAGGCACTTGACAG-3'

(Applied Biosystems). The related mRNA level was normalized to the β-actin mRNA level.

2.7. Western blot analysis

To obtain total protein, the lysis buffer containing protein was centrifuged at 12,000 *g* for 10 min. The protein concentration of the supernatant obtained was measured bicinchoninic acid (BCA) protein assay kit (Beyotime, P0009). The equal amounts of total proteins were separated by sodium dodecyl sulfate polyacrylamide gel electrophoresis and separated proteins were transferred onto polyvinylidene difluoride membrane filter (PVDF; Immobilon). The membrane was blocked with 3% BSA in TBST buffer for 2 h at room temperature. Next, the blot was incubated with corresponding primary antibody (anti-LC3,1:1000; anti-p62, 1:1000; anti-ACTB, 1:2000; anti-p-MTOR, 1:1000; anti-c-c3,

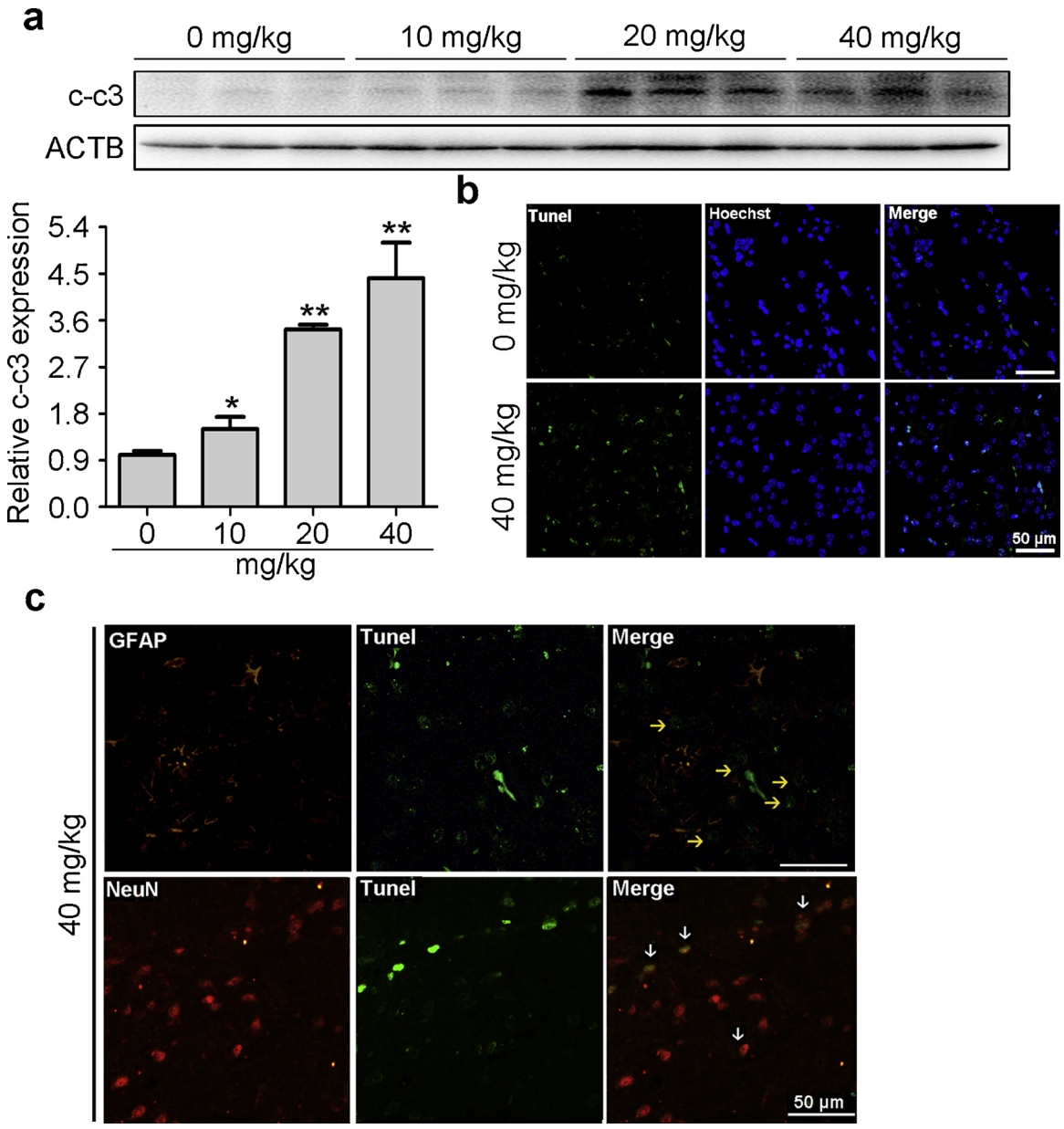

Fig. 1. Antimony (Sb) triggers neuronal apoptosis in mice. (a) Mice were treated with different doses of Sb for 4 weeks, followed by measurement of cleaved caspase 3 protein of brain tissue by Western blot. Quantification shown below represents the relative c-c3 expression level. (b) Tunel staining in the brain of mice exposed to 0 or 40 mg/kg Sb. (c) The colocalization of Tunel and astrocyte marker (GFAP) or neuron marker (Neu) in brain tissue of Sb-treated mice at 40 mg/kg. Yellow arrows show Tunel-positive cells without GFAP staining, while white arrows represent Tunel-positive neuros. All quantitative data are showed as means ± SD. n = 5. $^{**}P < 0.01$. $^{*}P < 0.05$. Scale bars: 50 μm.

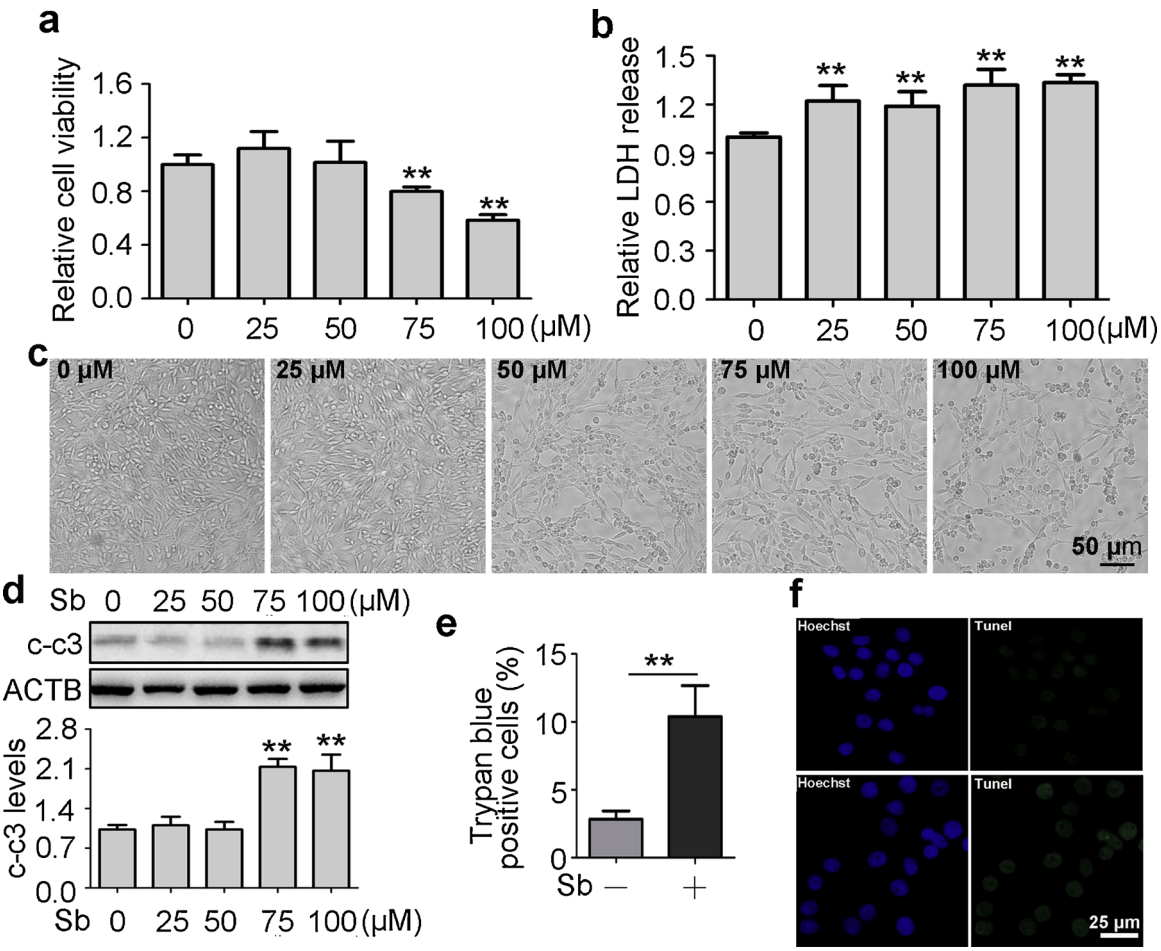

Fig. 2. Sb stimualtes apoptosis in PC12 cells. (a) PC12 cells were treated with Sb at indicated concentrations of for 24 h, and cell viability was measured by CCK-8. (b) PC12 cells were exposed to Sb as indicated in (a), then the LDH release in medium was assessed and normalized to control. (c) PC12 cells treated with Sb as indicated in (a) were imaged by an optical microscope (DM4000B, Leica). Scale bars: 50 μm. (d) PC12 cells were exposed to Sb as indicated in (a), followed by measurement of c-c3 expression levels by western blot. Quantification shown below represents the relative c-c3 expression level compared to control. (e) The PC12 cells was exposed to Sb (100 μM for 24 h), and the cell viability was measured by trypan blue. (f) The PC12 cells was exposed to Sb as indicated in (e), and the cellular apoptosis was detected by Tunel, Scale bars: 25 μm. All quantitative data are showed as means ± SD. $^{**}P < 0.01$. $^{*}P < 0.05$.

1:1000) at 4 °C overnight followed by incubation with HRP conjugated secondary antibody (Goat anti-Mouse, Li−COR Biosciences, B80908-02, 1:20,000; or Goat anti-Rabbit, Li−COR Biosciences, B81009-02, 1:20,000) for 1 h. Immunocomplex was detected by using an Enhanced Chemiluminescence system (ECL, Millipore, P90720). The intensity of relative protein expression was measured by densitometry (Image *J*).

2.8. Immunofluorescent staining

After Sb treatment, cells grown on coverslips were fixed with 4% paraformaldehyde in PBS at 4 °C for 1 h. After washed three times with ice-cold PBS, the cells were permeabilized with 0.5% Triton X-100 in PBS for 15 min and blocked at room temperature for 2 h with 5% normal goat serum. Cells were then incubated overnight at 4 °C with anti-LC3 antibodies (1:200 dilution in PBS) or anti-p62 antibodies (1:200 dilution in PBS). After incubation with the primary antibody, the cells were also washed 3 times followed by incubation with a mixture of tetramethyl rhodamin isothiocyanate fluorochrome-conjugated secondary antibodies (Invitrogen, 1:1000) for 1 h and Hoechst for 15 min at room temperature. At last, the treated cells were visualized using a fluorescent microscope (Leica, Microsystems, GmbH, Germany)

2.9. Sections and immunohistochemistry

Immunohistochemistry was used to evaluate the expression of LC3 and p62 in the brain slices. Briefly, the brain tissue slice were deparaffinized and rehydrated, done antigen retrieval in 10% sodium citrate buffer solution, and blocked endogenous peroxidase with 3% H_2O_2 solution for 20 min at room temperature. After completing the above steps, the slides were blocked in 3% BSA at room temperature for 2 h. Next, the sections was incubated with anti-LC3 antibody or anti-p62 antibody at 4 °C overnight followed by corresponding secondary antibody for 1 h. Finally, after treatment with DAB and hematoxylin, the brain tissue slice were rehydrated and were visualized using a microscope (Leica, Microsystems, GmbH, Germany).

2.10. Terminal deoxynucleotidyl transferase dUTP nick end labeling (tunel)

Apoptosis was determined by the TUNEL assay using the Dead End TM Fluorometric TUNEL System Kit (Promega, USA) as reported priviously (Jiao et al., 2019). Briefly, after treated by Sb, cells grown on coverslips were fixed with 4% paraformaldehyde in PBS at 4 °C for 25 min. After washed two times with ice-cold PBS, the cells were permeabilized with 0.2% Triton X-100 in PBS for 5 min and eguilibrated at room temperature for 10 min with 100 μl Equilibration Buffer. After equilibration, 50 μl rTdT incubation buffer (including 44 μl of EB, 5 μl of Nucleotide Mix as well as 1 μl rTdT enzyme) was added to react for 60 min at 37 °C. After removing the plastic coverslips, 2 × SSC buffer was added followed by incubation for 15 min at room temperature. After washed three times with PBS, the cells were incubated with

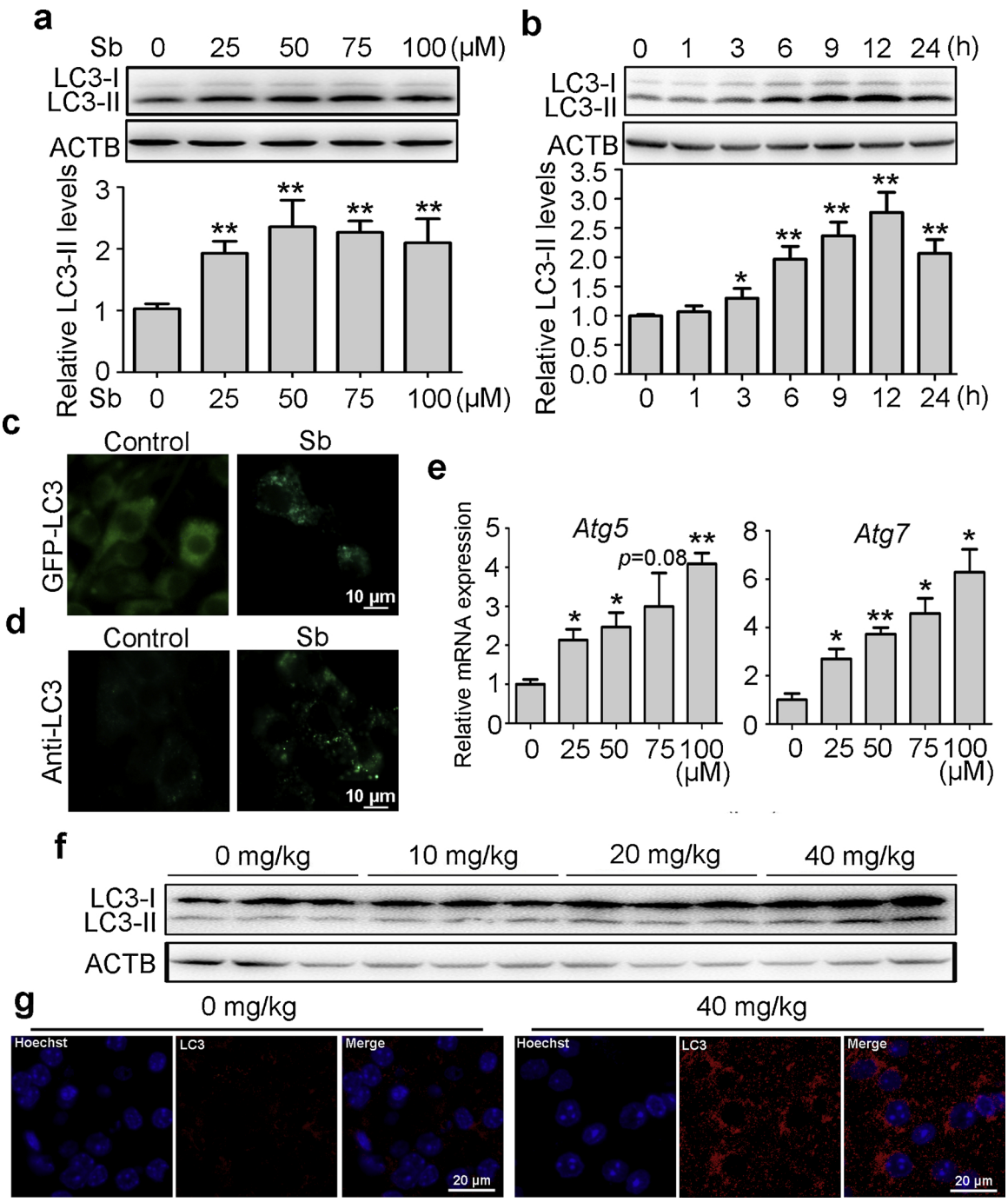

Fig. 3. Sb stimulates autophagosome accumulation in PC12 cells and mice brain. (a) PC12 cells were treated with different concentrations of Sb for 24 h, and the cellular LC3 expression levels were detected by Western blot. Quantification assay of relative LC3-II was shown below. (b) PC12 cells were exposed to Sb at 100 μM for different time as indicated, followed by detection of cellular LC3 expression levels by Western blot. Quantification assay of relative LC3-II was shown below. (c) PC12 cells transiently expressing GFP-LC3 were exposed to Sb at 100 μM for 24 h, then imaged by immunofluorescence microscopy. Scale bar: 10 μm. (d) PC12 cells were treated with Sb at 100 μM for 24 h, and the cellular LC3 dots was imaged by indirect immunofluorescence (IF) assay. Scale bar: 10 μm. (e) PC12 cells were treated with different doses of Sb for 24 h, and the levels of *Atg5* and *Atg7* were determined using qRT-PCR. (f, g) Mice were treated with different doses of Sb for 4 weeks, then LC3 protein expression levels of brain tissue were detected by Western blot (f), or IF (g). Scale bar: 20 μm. n = 5. All quantitative data are showed as means ± SD. $^{**}P < 0.01$. $^{*}P < 0.05$.

Hoechst for 15 min and visualized using a microscope (Leica, Microsystems, GmbH, Germany).

2.11. Measurement of malondialdehyde (MDA)

MDA is a natural product of lipid oxidation which occurs after oxidative stress, therefore its level could reflect lipid oxidation. In present study, the production of MDA was assessed by the MDA assay kit (Nanjing Jiancheng) according to the manufacturer's instruction. Before starting the experiment, four tubes were prepared as follows: 0.1 mL tetraethoxypropane at 10 nmol/ml was added in standard tube, 0.1 mL absolute ethanol was added in blank tube, 0.1 mL samples was added in measuring tube, 0.1 mL control samples was added in control tube. Then, 0.1 mL reagent one was added in above four tubes. Next,

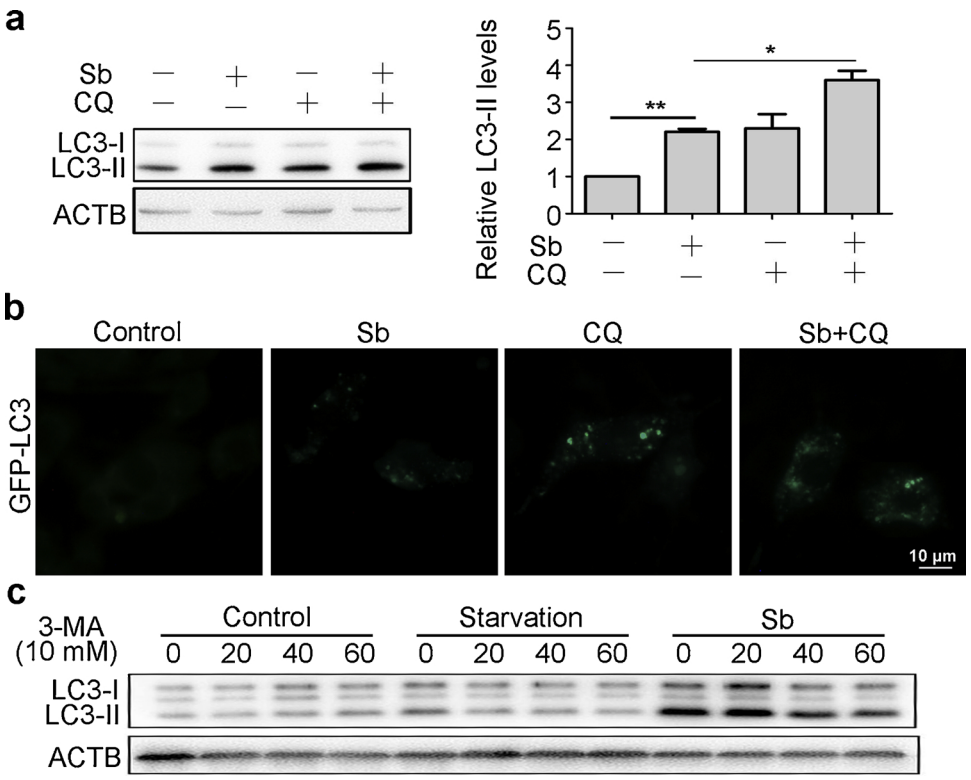

Fig. 4. Sb enhances autophagic flux in PC12 cells. (a) PC12 cells exposed to Sb were treated with or without pre-treated by 10 μM CQ, and the LC3 protein levels were detected by Western blot. Quantification shown right represents the relative LC3-II expression level compared to control. (b) PC12 cells transiently expressing GFP-LC3 were treated as indicated in (a), and imaged by immunofluorescence microscopy. Scale bars: 10 μm. (c) PC12 cells treated with 100 μM Sb for 24 h or starvation, were treated with 10 mM of 3-MA to block the formation of new autophagosomes, followed by measurement of LC3 expression levels by Western blot at the indicated time points. All quantitative data are presented as means ± SD, $^{**}P < 0.01$, $^{*}P < 0.05$.

3 mL reagent two was added for all tubes, followed by in addition of 1 mL reagent three in standard tube, blank tube, measuring tube. In control tube, 1 mL 50% glacial acetic acid was added. All the tubes were bathed at 95 °C for 40 min. After cooling, the tubes were centrifuged at 3500–4000 rpm for 10 min. The absorbance was measured at a test wavelength of 532 nm and calculated MDA activity according to formula.

2.12. Measurement of lactate dehydrogenase (LDH) release

LDH is a stable protein that is present in the cytoplasm of normal cells. It is released once the cell membrane is damaged. Therefore, the release of LDH in medium is used as a indicator of cell damage. Here, The release of LDH was measured in the culture supernatants by measuring the LDH activity with the LDH assay kit (Nanjing Jiancheng) following the manufacturer's instructions. Four tubes were prepared as follows: 1) blank tube: 25 μl double distilled water and 25 μl matrix buffer; 2) standard tube: 5 μl double distilled water, 20 μl 0.2 mM pyruvic acid standard application solution and 25 μl matrix buffer; 3) measuring tube: 20 μl collected culture supernatants, 25 μl matrix buffer, 5 μl coenzyme one application solution; 4) control tube: 20 μl collected culture supernatants, 25 μl matrix buffer, 5 μl double distilled water. Then, four tubes was incubated at 37 °C for 15 min, then added 25 μl 2,4-dinitrophenylhydrazine for another incubation at 37 °C for 15 min. Next, 250 μl 0.4 mM NaOH was added and incubated at room temperature for 5 min. The absorbance was measured at a test wavelength of 450 nm and calculated LDH activity according to formula.

2.13. Statistical analysis

Results are expressed as mean ± SD for at least three independent experiments. Kolmogorov-Smirnov test was applied to data distribution assay. Then, student's *t*-test or analysis of variance (ANOVA) was used for statistical analysis of normal distribution, and Wilcoxon Rank-Sum test was used for statistical analysis of unnormal distribution. A probability value of 0.05 or less was considered to be significant.

3. Results

3.1. Sb exposure induces neuronal cell apoptosis

Neuronal cell death plays a major role during environmental pollutant-associated neurotoxicity. We therefore determined whether Sb induced neuronal death in Sb-exposed mice brain cortex tissue. Fig. 1a shows that Sb increased the activation of caspase, as indicated by the dose-dependent increase cleaved caspase 3 (Fig. 1a). We also observed an increased number of Tunel-positive cells in mice exposed to 40 mg/kg Sb, confirming Sb-induced cell apoptosis in the brain (Fig. 1b). We then conducted double stain analysis of Tunel with different phenotypic markers, including GFAP (an astrocyte marker) and NeuN (a neuron marker), and found that Sb triggered apoptosis predominantly in neurons rather than astrocytes (Fig. 1c). We subsequently used PC12 cells, a valuable model for research on neuronal toxicity, to characterise the molecular mechanism of Sb-induced neuronal apoptosis.

In vitro, Sb decreased cell viability in a dose-dependent way (Fig. 2a). To further investigate the effects of Sb on PC12 cells, a lactate dehydrogenase (LDH) assay, another indicator of cell toxicity, was performed. The results showed that LDH release was also elevated in a dose-dependent manner (Fig. 2b). Interestingly, 25 and 50 μM Sb increased LDH release, while failed to decrease cell viability. Furthermore, bright field images of PC12 cells treated with Sb showed a dramatically increased number of apoptotic cells (Fig. 2c). Exposure to Sb led to increased caspase activation upon 75 and 100 μM Sb treatment (Fig. 2d). Moreover, we chosed treatment with Sb at 100 μM for further assay. Trypan blue staining showed decreased cell viability after Sb exposure (Fig. 2e). Tunel-positive cells was increased in Sb-treated cells, indicating that Sb induced neuronal apoptosis (Fig. 2f).

3.2. Sb triggers autophagy in PC12 cells and mice brain tissue

To explore whether autophagy was stimulated following Sb exposure in PC12 cells, we determined the protein expression of microtubule-associated protein 1 light chain 3, an autophagosome marker,

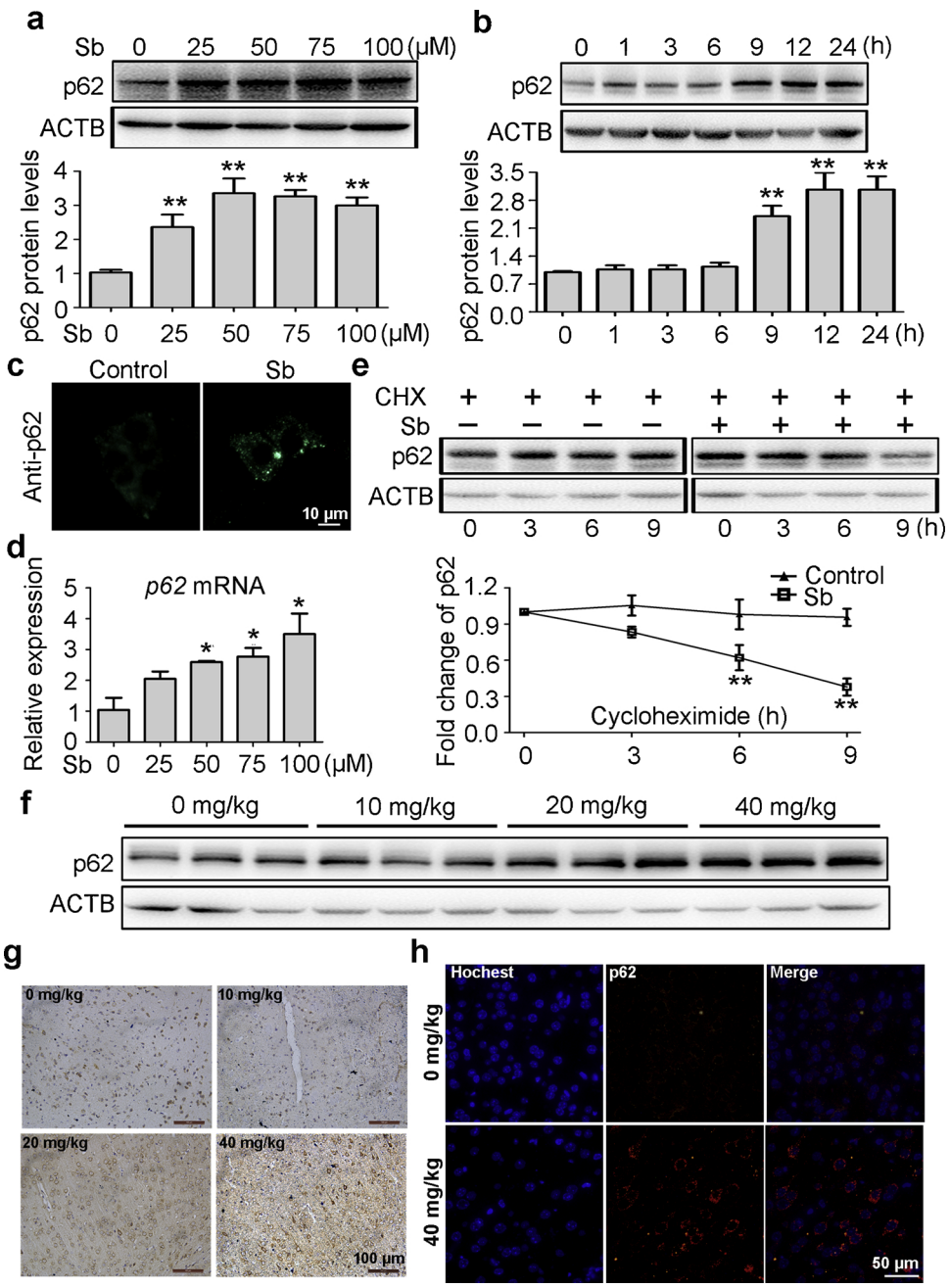

Fig. 5. Sb enhances p62 expression and protein degradation. (a) PC12 cells were treated with different concentrations of Sb for 24 h, and the cellular p62 expression levels were detected by Western blot. The graph below shows a statistical analysis of p62/ACTB *versus* the control. (b) PC12 cells were exposed to Sb at 100 μM for different time as indicated, followed by detection of cellular p62 expression levels by Western blot. The graph below shows a statistical analysis of p62/ACTB *versus* the control. (c) PC12 cells were exposed to Sb at 100 μM for 24 h, then the p62 dots were imaged by indirect immunofluorescence assay. Scale bar: 10 μm. (d) PC12 cells were treated with different doses of Sb for 24 h, and the levels of *p62* were determined using qRT-PCR. (e) We co-cultured Sb with 10 μM cycloheximide (CHX) for the indicated times. Western blot was used for p62 expression analysis. The graph below illustrates the statistical analysis of p62/ACTB *versus* the 0 h. (f, g) Mice were treated with different doses of Sb for 4 weeks, then p62 protein expression levels of brain tissue were detected by Western blot (f) or IHC (g). Scale bar: 100 μm. (h) Mice was treated with or without Sb at 40 mg/kg, then the p62 dots was measured by IF. Scale bar: 50 μm. All quantitative data are presented as means ± SD, n = 5. $^{**}P < 0.01$, $^{*}P < 0.05$.

using western blotting, and found that LC3-II expression was increased in Sb-treated cells in both a dose-dependent and time-dependent manner (Fig. 3a and b). Consistently, increased green fluorescent protein (GFP)-tagged LC3 dots were found in GFP-LC3-expressing PC12 cells treated with 100 μM Sb for 24 h (Fig. 3c). In a similar manner, immunofluorescence staining revealed more LC3-positive punctuated structures in PC12 cells after the above-mentioned treatment (Fig. 3d). We then measured the expression levels of two important autophagy associated genes, *Atg5* and *Atg7*, using qRT-PCR. Sb treatment for 24 h upregulated their expression levels (Fig. 3e). We further conducted an *in vivo* study, which showed that LC3-II expression was gradually upregulated as the Sb concentration increased from 0 to 40 mg/kg (Fig. 3f), accompanied by increased LC3 dots shown by immunofluorescence staining (Fig. 3g).

3.3. Sb enhances autophagic flux and p62 expression

LC3-II protein upregulation can result from not only autophagy induction, but also from autophagic flux blockage. To measure autophagic flux, we determined the LC3-II protein expression levels in the absence or presence of chloroquine (CQ), a common autophagy inhibitor. We found that 10 μM CQ treatment resulted in further increases in LC3-II levels, when compared with the single Sb-treated group (Fig. 4a). A similar result was seen using GFP-LC3 puncta in PC12 cells, suggesting that Sb enhanced the autophagic flux (Fig. 4b). Furthermore, once autophagosome synthesis was inhibited by 3-methyladenine, the LC3-II protein was gradually degraded in Sb-treated cells, providing evidence of normal autophagic degradation (Fig. 4c).

To further confirm that Sb accelerated autophagic flux, we detected the protein sequestosome 1 (p62), a classic substrate degraded by autophagy. Unexpectedly, the results showed that Sb caused its increase rather than decrease in a dose- and time-dependent manner (Fig. 5a and

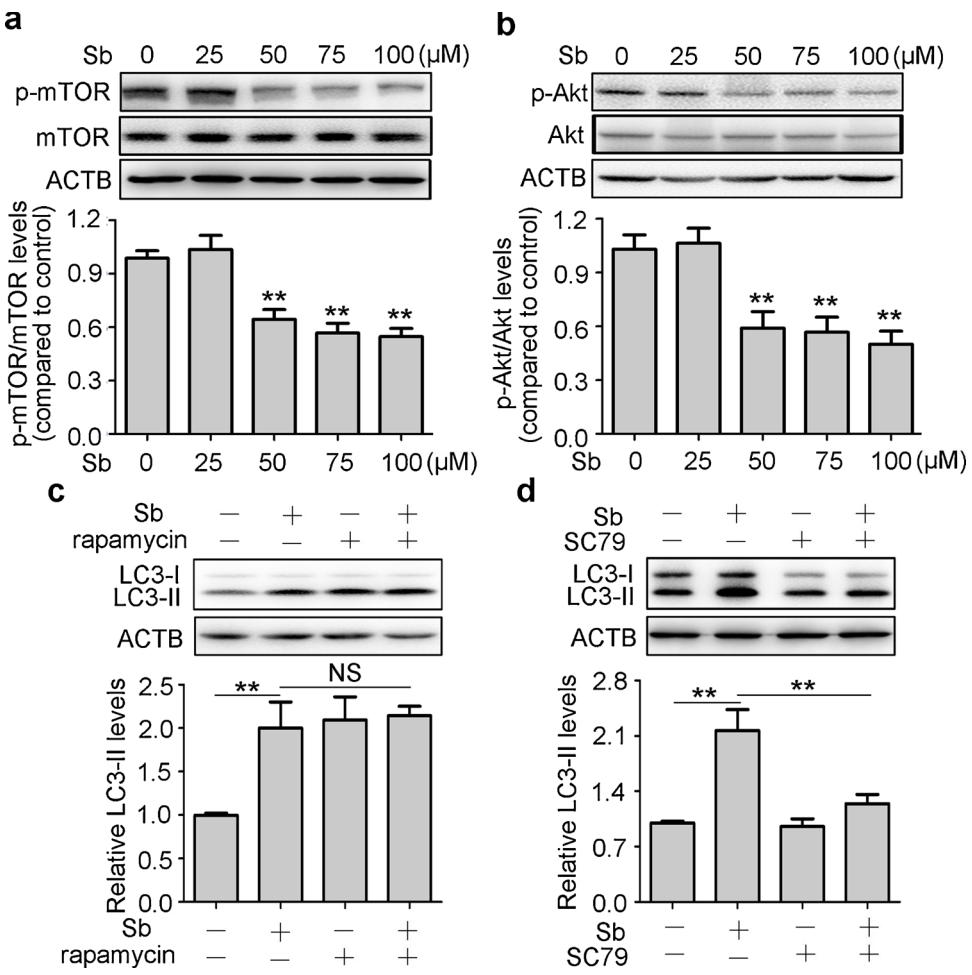

Fig. 6. Akt/mTOR pathway inhibition is involved in Sb-induced autophagy. (a) PC12 cells were treated with Sb at indicated doses for 24 h, and the p-mTOR as well as mTOR expression levels were detected by Western blot. The graph below shows a statistical analysis of p-mTOR/mTOR *versus* the control. (b) PC12 cells were treated with Sb at indicated in (B), and the p-Akt as well as Akt expression levels were detected by Western blot. The graph below shows a statistical analysis of p-Akt /Akt *versus* the control. (c) PC12 cells exposed to Sb were treated with or without pretreated by 300 nM rapamycin, and the LC3 protein levels were detected by Western blot. Quantification assay of relative LC3-II was shown below. (d) PC12 cells pre-treated with or without 5 μg/ml SC79 (Akt activator) for 1 h were exposed to 100 μM Sb for 24 h. The LC3 expression levels were detected by Western blot. Quantification assay of relative LC3-II was shown below. All quantitative data are presented as means ± SD, $^{**}P < 0.01$, NS: no significance.

b), and that the p62 protein was assembled into aggregates in Sb-treated cells (Fig. 5c). Furthermore, qRT-PCR results showed that p62 mRNA was dramatically upregulated, demonstrating increased p62 protein levels due to enhanced expression (Fig. 5d). Next, we directly tested p62 protein degradation using cycloheximide pretreatment, which is a protein synthesis inhibitor (Fig. 5e). The results showed that p62 degradation was accelerated in Sb-treated cells, in accordance with enhanced autophagic flux as shown in Fig. 4. To verify our *in vitro* findings, we examined p62 in Sb-treated mice. Both immunoblotting and immunohistochemical assays showed increased p62 protein levels in brain tissues (Fig. 5f and g). Similarly, more p62 dot accumulation was observed in Sb-exposed mice brains (Fig. 5h). Taken together, the results demonstrated that Sb treatment resulted in enhancement of autophagic flux, protein degradation, and mRNA expression of p62.

3.4. Sb induces autophagy through ROS-mediated inactivating Akt/mTOR signaling

We then characterised the underlying molecular mechanism involved in Sb-induced autophagy in neuronal cells. We especially characterised the Akt/mTOR pathway because of its critical role in autophagy regulation. Immunoblotting was used to assess the expression levels of p-mTOR, mTOR, p-Akt, and Akt in PC12 cells following exposure to Sb. Fig. 6a and b show that treatment with Sb led to significant reduction in the phosphorylation levels of mTOR and Akt in a dose-dependent manner, suggesting that inhibition of the Akt/mTOR pathway may be involved in Sb-induced autophagy in PC12 cells (Fig. 6a and b). To confirm this possibility, we treated cells with Sb and rapamycin to evaluate their combined effect. Rapamycin failed to synergistically increase the production of LC3-II in Sb-treated cells, suggesting that Sb-stimulated production of autophagosomes occurred through an mTOR inhibition-dependent pathway (Fig. 6c). Next, we assessed the effect of the Akt activator (SC79) on Sb-induced autophagy activation. Fig. 6d shows that PC12 cells treated with SC79 showed significant inhibition of autophagy induction compared with Sb treatment alone (Fig. 6d).

Oxidative stress, especially ROS generation, has been implicated in Akt/mTOR pathway inhibition and subsequent autophagy activation. Fig. 7a shows that Sb treatment dramatically increased the cellular ROS levels in a dose-dependent manner in PC12 cells. The cellular levels of malondialdehyde were also significantly increased in cells treated as described in Fig. 7a (Fig. 7b). We examined the effects of N-acetylcysteine (NAC), a ROS scavenger, on Sb-induced autophagy and cell death. The results showed that NAC protected PC12 cells from Sb-induced cell viability loss (Fig. 7c). Moreover, the phosphorylation levels of Akt and mTOR were significantly increased in Sb-exposed cells following NAC treatment (Fig. 7d). NAC also increased the mRNA levels of Atg5 and Atg7, as well as p62 and LC3-II protein levels in Sb-treated PC12 cells (Fig. 7e and f). Collectively, our data indicated that Sb-induced autophagy in PC12 cells was a result of ROS-mediated Akt/mTOR pathway inhibition.

3.5. Autophagy mediated Sb-induced neuronal apoptosis

To observe autophagy function in Sb-mediated neuronal apoptosis, CQ was used to inhibit the late stage of autophagy. The results showed a significant increase in cell viability following treatment with CQ (Fig. 8a). Similarly, CQ reduced LDH release in Sb-treated PC12 cells

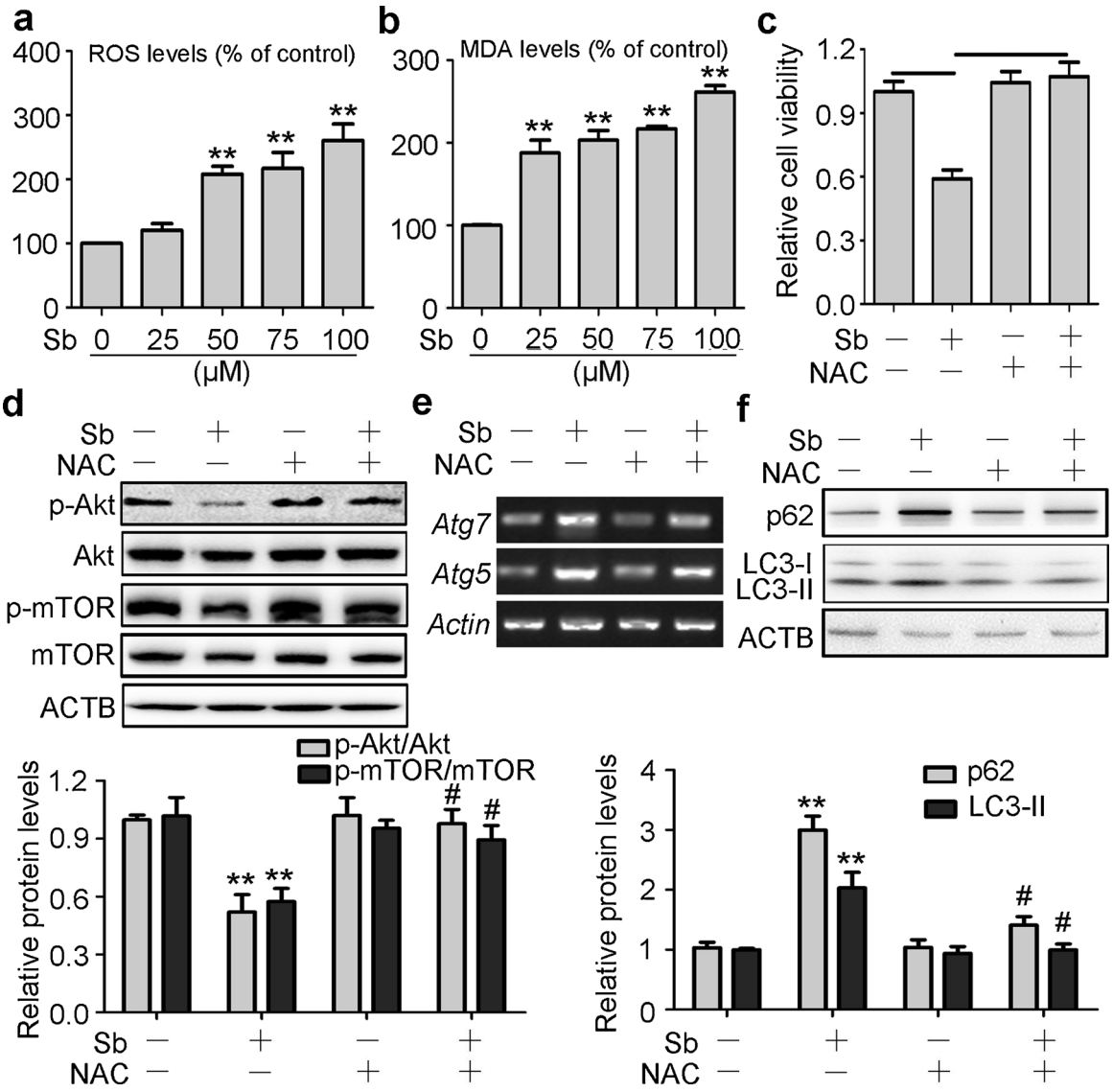

Fig. 7. ROS mediated Sb-induced Akt/mTOR pathway inhibition and subsequent autophagy. (a) PC12 cells were exposed to Sb as indicated doses for 24 h, then the ROS was detected by DCFH-DA, and normalized to control. (b) The MDA levels of PC12 cells exposed to Sb as indicated in (a) were measured, and normalized to control. (c) PC12 cells treated with or without pre-treated by 5 mM NAC for 1 h were exposed to 100 μM Sb for 24 h, and cell viability was measured by CCK-8. (d) PC12 cells treated with or without pre-treated by 5 mM NAC for 1 h were exposed to 100 μM Sb for 24 h, and p-Akt, Akt, p-mTOR, mTOR protein expression were measured by Western blot. The graph below shows a statistical analysis of p-Akt/Akt and p-mTOR/mTOR. (e, f) PC12 cells treated as in (d), then *Atg5* as well as *Atg7* were determined using a semi-quantitative PCR (e), and LC3 as well as p62 protein expression levels were measured by Western blot (f), the graph below shows a statistical analysis of p62/ACTB and LC3-II/ACTB. All quantitative data are presented as means ± SD. $^{**}P < 0.01$ *vs* control, $^{\#\#} P < 0.05$ *vs* Sb-treated group.

(Fig. 8b). CQ treatment was also found to decrease Sb-induced PC12 cell apoptosis, as indicated by reduced caspase activation (Fig. 8c). In Sb-exposed mice brain tissue, most Tunel positive cells showed more LC3 or p62 expression compared with Tunel negative cells, implying that autophagy induction triggered apoptosis as a result of Sb treatment (Fig. 8d). Taken together, these results showed that autophagy induction functioned as a proapoptotic mechanism in Sb-associated neuronal damage.

4. Discussion

Sb, a toxic trace element, has been found in the human brain, and has been associated with abnormal behaviour of mice. However, no study has investigated the cellular outcomes and molecular mechanisms of Sb-associated neurotoxicity. The present study confirmed that Sb induced neuronal apoptosis, providing the first cellular evidence of the involvement of neurotoxicity following Sb exposure. Furthermore, we found that Sb exposure resulted in proapoptotic autophagy activation accompanied by Akt/mTOR pathway inhibition, and that an Akt activator alleviated Sb-induced autophagy. Importantly, ROS blockage ameliorated Sb-triggered inhibition of the Akt/mTOR pathway and subsequent autophagy induction as well as cell death. Overall, our data provides the first molecular evidence of the mechanism of Sb-induced neurotoxicity, showing Sb induced ROS-mediated autophagy activation by inhibiting the Akt/mTOR pathway, thereby leading to neuronal apoptosis.

The role of autophagy as a causative or protective factor and even as a consequence of AD is not yet completely known (Zare-Shahabadi et al., 2015). Decreased autophagy can contribute to the accumulation of tau and Aβ (Menzies et al., 2017). For example, genetic reduction of beclin-1 expression results in increased Aβ accumulation and neurodegeneration. Furthermore, rapamycin, a classic mTOR inhibitor, reduces Aβ and tau pathology and improves cognition-dependent autophagy induction, suggesting that autophagy plays a protective role

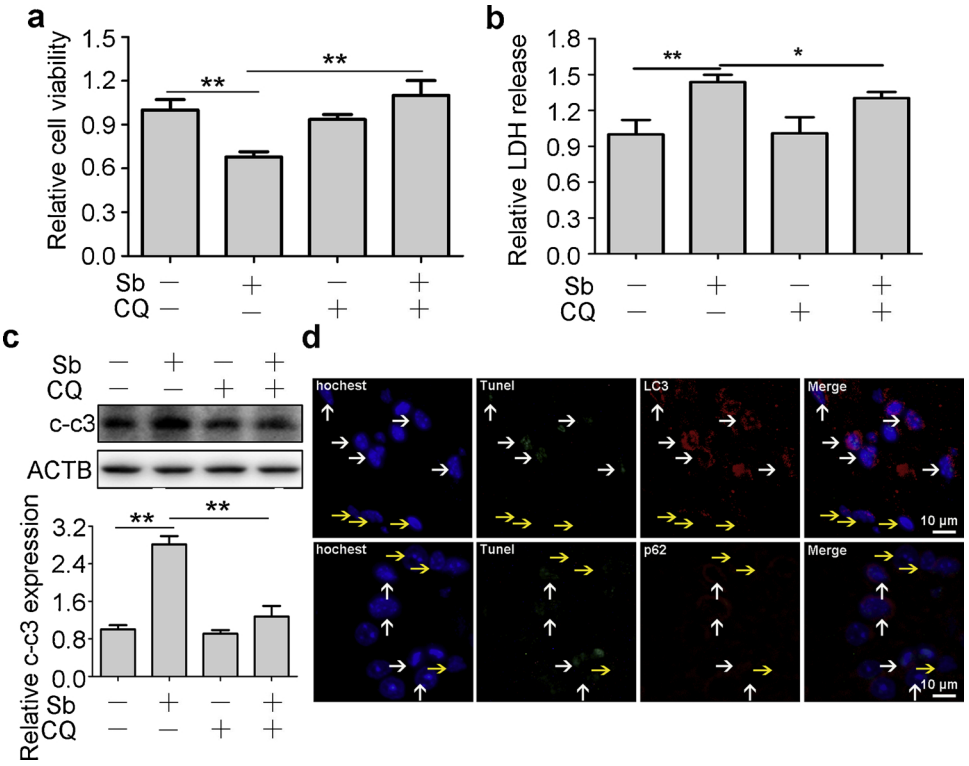

Fig. 8. Autophagy mediated Sb-induced neuronal apoptosis. (a) PC12 cells treated with or without pre-treated by 10 μM CQ were exposed to 100 μM Sb for 24 h, and cell viability was measured by CCK-8. (b) PC12 cells were treated as indicated in (a), then the LDH release was assessed and normalized to control. (c) PC12 cells were treated as indicated in (a), followed by c-c3 expression assay by wb. The bottom panels show the statistics for relative cleaved caspase3 protein level. (d) The co-location of Tunel with LC3 or p62 in Sb-exposed mice brain. White arrows: Tunel-postive cells with LC3 or p62 staining. Yellow arrow: Tunel-negative cells without LC3 or p62 staining. Scale bar: 10 μm. n = 5. All quantitative data are presented as means ± SD, $^{**}P < 0.01$, $^{*}P < 0.05$.

(Cai and Yan, 2013; Spilman et al., 2010). However, increased autophagy induction is relatively frequent in neurodegenerative diseases. Autophagy itself may cause Aβ secretion, while Aβ production was decreased by 90% in autophagy-deficient mice, indicating that autophagy activation also acts as a pathological mechanism (Hamano et al., 2018). Collectively, autophagy is implicated in AD, although it is a double-edged sword because of its functions in cell protection or destruction, depending on the cell type and exposure, once activated. In the present study, we found that neuronal autophagy activation triggered apoptosis, a critical cellular mechanism of AD, supporting the hypothesis that excessive autophagy may act as a causative factor for Sb-associated AD risk. Autophagy-deficient mice exposed to Sb could therefore be used to identify the role of autophagy in Sb-induced neurotoxicity.

Generally, autophagy regulation could be mTOR-dependent or mTOR-independent (Antonioli et al., 2017). In our previous study, we reported that Sb induced autophagy *via* a ROS-mediated process independent of mTOR inhibition in A549 cells (Zhao et al., 2017). However, in the present study, we showed that Sb stimulated ROS-mediated autophagy in an Akt/mTOR-dependent manner in PC12 cells. Our findings indicated that Sb triggered a cell type-dependent regulation of autophagy. In both cases, p62 was increased rather than decreased due to upregulated mRNA expression, although autophagic flux was accelerated. When considering the antioxidant response element in the p62 promoter, NF-E2-related factor 2 (Nrf2) could function *via* binding the antioxidant response element to promote p62 transcription. It should also be noted that Nrf2 was activated by Sb, and protected against cellular apoptosis by repressing ROS production (Jiang et al., 2016). Furthermore, p62 possesses other roles independent of autophagy, such as the regulation of inflammation and apoptosis (Choe et al., 2014; Fan et al., 2018). Additional studies on the biological outcomes of Sb-induced p62 upregulation are therefore urgently needed.

Our results provided evidence of neuronal apoptosis, a critical cellular outcome in AD following Sb exposure. We therefore hypothesised that Sb exposure is a risk factor for AD. This hypothesis is supported by the following data. Sb exposure by intraperitoneal injection leads to impaired cognitive function, an important AD clinical symptom, as shown by the Morris water maze test (Piirainen et al., 2017; Tanu et al., 2018). Moreover, several molecular mechanisms involved in AD are related to Sb exposure. Oxidative stress, as well as the Akt signalling pathway, is essential in AD (Matsuda et al., 2018). AD shows an increase of neurofibrillary plaques in the brain, consisting of hyperphosphorylated tau and abnormal amyloid-β isoforms. As a kinase implicated in tau hyperphosphorylation in AD, GSK-3β could be activated by abnormal Akt signalling. Downregulation of Akt, contributing to elevated GSK-3β activity, may be involved in the pathogenesis of AD (Hernandez et al., 2013). The results of the present study showed that Sb treatment resulted in the downregulation of Akt activation and thus led to autophagy *via* the generation of ROS. Further investigations on the role of Akt suppression in Sb-induced neurotoxicity are urgently needed. Most reports have failed to find differences in Sb concentrations in the serum or plasma and cerebrospinal fluid between AD patients and healthy subjects (Alimonti et al., 2007; Bocca et al., 2005; Gerhardsson et al., 2008). The association of Sb exposure and AD should be detected in occupational exposure individuals. More importantly, to confirm the AD risk from Sb exposure, additional studies should be performed to characterise the effects of Sb on AD-like pathologies, as well as to determine its underlying mechanism of action.

In summary, this is the first report identifying the molecular mechanism responsible for Sb-associated neurotoxicity, which showed that Sb exposure induced neuronal apoptosis *in vitro* and *in vivo* through ROS-mediated Akt/mTOR pathway inhibition and autophagy activation. These findings provide a novel mechanism by which Sb triggers neuronal damage. Furthermore, these results may provide the basis for new strategies to prevent Sb-induced neurotoxicity by inhibiting ROS and autophagy.

Acknowledgments

This work was supported by the National Natural Science Foundation of China (81703255); Nantong Jiangsu scientific research project (MS12017014-8); Scientific Research Project of Wuxi Health and Family Planning Commission (Q201733) and The Yong Medical Talents of wuxi (QNRC036).

References

Alimonti, A., Ristori, G., Giubilei, F., Stazi, M.A., Pino, A., Visconti, A., Brescianini, S., Sepe Monti, M., Forte, G., Stanzione, P., et al., 2007. Serum chemical elements and oxidative status in Alzheimer's disease, Parkinson disease and multiple sclerosis. Neurotoxicology 28, 450–456.

Antonioli, M., Di Rienzo, M., Piacentini, M., Fimia, G.M., 2017. Emerging mechanisms in initiating and terminating autophagy. Trends Biochem. Sci. 42, 28–41.

Bocca, B., Forte, G., Petrucci, F., Pino, A., Marchione, F., Bomboi, G., Senofonte, O., Giubilei, F., Alimonti, A., 2005. Monitoring of chemical elements and oxidative damage in patients affected by Alzheimer's disease. Ann. Ist. Super. Sanita 41, 197–203.

Cai, Z., Yan, L.J., 2013. Rapamycin, autophagy, and alzheimer's disease. J. Biochem. Pharmacol. Res. 1, 84–90.

Caricchio, V.L., Sama, A., Bramanti, P., Mazzon, E., 2018. Mercury involvement in neuronal damage and in neurodegenerative diseases. Biol. Trace Elem. Res.

Cho, Y.E., Lee, M.H., Song, B.J., 2017. Neuronal cell death and degeneration through increased nitroxidative stress and tau phosphorylation in HIV-1 transgenic rats. PLoS One 12, e0169945.

Choe, J.Y., Jung, H.Y., Park, K.Y., Kim, S.K., 2014. Enhanced p62 expression through impaired proteasomal degradation is involved in caspase-1 activation in monosodium urate crystal-induced interleukin-1b expression. Rheumatology (Oxford) 53, 1043–1053.

Dribben, W.H., Creeley, C.E., Farber, N., 2011. Low-level lead exposure triggers neuronal apoptosis in the developing mouse brain. Neurotoxicol. Teratol. 33, 473–480.

Engstrom, A., Wang, H., Xia, Z., 2015. Lead decreases cell survival, proliferation, and neuronal differentiation of primary cultured adult neural precursor cells through activation of the JNK and p38 MAP kinases. Toxicol. In Vitro 29, 1146–1155.

Fan, L., Yin, S., Zhang, E., Hu, H., 2018. Role of p62 in the regulation of cell death induction. Apoptosis 23, 187–193.

Fathabadi, B., Dehghanifiroozabadi, M., Aaseth, J., Sharifzadeh, G., Nakhaee, S., Rajabpour-Sanati, A., Amirabadizadeh, A., Mehrpour, O., 2018. Comparison of blood lead levels in patients with alzheimer's disease and healthy people. Am. J. Alzheimers Dis. Other Demen. 33, 541–547.

Fricker, M., Tolkovsky, A.M., Borutaite, V., Coleman, M., Brown, G.C., 2018. Neuronal cell death. Physiol. Rev. 98, 813–880.

Gerhardsson, L., Lundh, T., Minthon, L., Londos, E., 2008. Metal concentrations in plasma and cerebrospinal fluid in patients with Alzheimer's disease. Dement. Geriatr. Cogn. Disord. 25, 508–515.

Hamano, T., Hayashi, K., Shirafuji, N., Nakamoto, Y., 2018. The implications of autophagy in alzheimer's disease. Curr. Alzheimer Res.

Herath, I., Vithanage, M., Bundschuh, J., 2017. Antimony as a global dilemma: geochemistry, mobility, fate and transport. Environ. Pollut. 223, 545–559.

Hernandez, F., Lucas, J.J., Avila, J., 2013. GSK3 and tau: two convergence points in Alzheimer's disease. J. Alzheimers Dis. 33 (Suppl 1), S141–S144.

Hock, A., Demmel, U., Schicha, H., Kasperek, K., Feinendegen, L.E., 1975. Trace element concentration in human brain. Activation analysis of cobalt, iron, rubidium, selenium, zinc, chromium, silver, cesium, antimony and scandium. Brain 98, 49–64.

Jiang, X., An, Z., Lu, C., Chen, Y., Du, E., Qi, S., Yang, K., Zhang, Z., Xu, Y., 2016. The protective role of Nrf2-Gadd45b against antimony-induced oxidative stress and apoptosis in HEK293 cells. Toxicol. Lett. 256, 11–18.

Jiao, M., Yin, K., Zhang, T., Wu, C., Zhang, Y., Zhao, X., Wu, Q., 2019. Effect of the SSeCKS-TRAF6 interaction on gastrodin-mediated protection against 2,3,7,8-tetrachlorodibenzo-p-dioxin-induced astrocyte activation and neuronal death. Chemosphere 226, 678–686.

Kayed, R., Lasagna-Reeves, C.A., 2013. Molecular mechanisms of amyloid oligomers toxicity. J. Alzheimers Dis. 33 (Suppl 1), S67–S78.

Matsuda, S., Nakagawa, Y., Tsuji, A., Kitagishi, Y., Nakanishi, A., Murai, T., 2018. Implications of PI3K/AKT/PTEN signaling on superoxide dismutases expression and in the pathogenesis of Alzheimer's disease. Diseases 6.

Menzies, F.M., Fleming, A., Caricasole, A., Bento, C.F., Andrews, S.P., Ashkenazi, A., Fullgrabe, J., Jackson, A., Jimenez Sanchez, M., Karabiyik, C., et al., 2017. Autophagy and neurodegeneration: pathogenic mechanisms and therapeutic opportunities. Neuron 93, 1015–1034.

Morris, D.R., Levenson, C.W., 2017. Neurotoxicity of zinc. Adv. Neurobiol. 18, 303–312.

Pellacani, C., Costa, L.G., 2018. Role of autophagy in environmental neurotoxicity. Environ. Pollut. 235, 791–805.

Piirainen, S., Youssef, A., Song, C., Kalueff, A.V., Landreth, G.E., Malm, T., Tian, L., 2017. Psychosocial stress on neuroinflammation and cognitive dysfunctions in Alzheimer's disease: the emerging role for microglia? Neurosci. Biobehav. Rev. 77, 148–164.

Polanco, J.C., Li, C., Bodea, L.G., Martinez-Marmol, R., Meunier, F.A., Gotz, J., 2018. Amyloid-beta and tau complexity - towards improved biomarkers and targeted therapies. Nat. Rev. Neurol. 14, 22–39.

Smale, G., Nichols, N.R., Brady, D.R., Finch, C.E., Horton Jr, W.E., 1995. Evidence for apoptotic cell death in Alzheimer's disease. Exp. Neurol. 133, 225–230.

Spilman, P., Podlutskaya, N., Hart, M.J., Debnath, J., Gorostiza, O., Bredesen, D., Richardson, A., Strong, R., Galvan, V., 2010. Inhibition of mTOR by rapamycin abolishes cognitive deficits and reduces amyloid-beta levels in a mouse model of Alzheimer's disease. PLoS One 5, e9979.

Sundar, S., Chakravarty, J., 2010. Antimony toxicity. Int. J. Environ. Res. Public Health 7, 4267–4277.

Tanu, T., Anjum, A., Jahan, M., Nikkon, F., Hoque, M., Roy, A.K., Haque, A., Himeno, S., Hossain, K., Saud, Z.A., 2018. Antimony-induced neurobehavioral and biochemical perturbations in mice. Biol. Trace Elem. Res. 186, 199–207.

Xu, L., Zhang, W., Liu, X., Zhang, C., Wang, P., Zhao, X., 2018. Circulatory levels of toxic metals (Aluminum, cadmium, mercury, lead) in patients with alzheimer's disease: a quantitative meta-analysis and systematic review. J. Alzheimers Dis. 62, 361–372.

Yang, Y.W., Liou, S.H., Hsueh, Y.M., Lyu, W.S., Liu, C.S., Liu, H.J., Chung, M.C., Hung, P.H., Chung, C.J., 2018. Risk of Alzheimer's disease with metal concentrations in whole blood and urine: a case-control study using propensity score matching. Toxicol. Appl. Pharmacol. 356, 8–14.

Zare-Shahabadi, A., Masliah, E., Johnson, G.V., Rezaei, N., 2015. Autophagy in Alzheimer's disease. Rev. Neurosci. 26, 385–395.

Zhang, J., Cai, T., Zhao, F., Yao, T., Chen, Y., Liu, X., Luo, W., Chen, J., 2012. The role of alpha-synuclein and tau hyperphosphorylation-mediated autophagy and apoptosis in lead-induced learning and memory injury. Int. J. Biol. Sci. 8, 935–944.

Zhao, X., Xing, F., Cong, Y., Zhuang, Y., Han, M., Wu, Z., Yu, S., Wei, H., Wang, X., Chen, G., 2017. Antimony trichloride induces a loss of cell viability via reactive oxygen species-dependent autophagy in A549 cells. Int. J. Biochem. Cell Biol. 93, 32–40.